ELSEVIER

Chemical Engineering Journal 135S (2008) S259–S269

Chemical Engineering Journal

www.elsevier.com/locate/cej

Design of a mesh microreactor for even flow distribution and narrow residence time distribution

C. Amador [a], D. Wenn [b], J. Shaw [b], A. Gavriilidis [a], P. Angeli [a,*]

[a] *Department of Chemical Engineering, University College London, Torrington Place, London WC1E 7JE, UK*
[b] *Central Research Laboratories (CRL), Middlesex UB3 1HH, UK*

Abstract

Flow and residence time distributions are analysed in a microreactor where the reactant fluid phases come into contact through the microfabricated pores of a mesh. An analytical resistance network method that is based on the analogy of viscous flow to networks of electrical resistances, initially developed to analyse flow distribution in scale-out geometries, is applied to identify possible reactor plate geometries. The main assumptions of this method and the suggested reactor plate geometries are successfully validated via computational fluid dynamics simulations combined with a particle tracking methodology for the residence time distribution. The method is used to produce a reactor plate geometry that results in uniform residence time distribution within the active mesh region while minimising the non-active volume on the plate and the reactants' collecting channel, which affect the overall residence time distribution as well as the time for flushing/emptying the reactor. Experimental tests carried out to visually assess flow distribution in different plate geometries qualitatively agree with the theoretical results.

Keywords: Microreactor; Resistance network model; Residence time distribution

1. Introduction

Microreactors enhance heat/mass transfer by promoting contact between very thin fluid reactant layers and are a powerful tool for process intensification. The mesh microreactor developed by CRL [1] (see Fig. 1) is utilised to carry out two-phase reactions [2] by bringing the two phases into contact via a mesh with microfabricated straight pores which offers increased stability and large open interfacial area between the two reacting phases (up to 45%). Since the two phases are kept separate there are no issues of phase separation at the end of the reactor. The system is intended for screening of fluid–liquid reactions sequentially in both batch and flow-through modes.

In the present work, an analytical resistance network model (RNM), developed by [3] for uniform flow distribution in scale-out geometries, is adapted to study and improve flow distribution in the mesh microreactor. Even flow distribution along the reaction plate improves reaction selectivity and efficiency by narrowing the residence time distribution (RTD). The results are compared with those from accurate numerical simulations of the flow field on the reactor plate and from particle tracking methodology for RTD. Improvements on the current design are suggested that achieve even flow distribution and minimise sample dispersion.

1.1. Residence time distribution analysis

Residence time distributions are generally utilised to understand the flow patterns inside a reactor. Two different systems may have similar mean residence time but very different RTD, which may impact reaction conversion and selectivity. The RTD is experimentally obtained by injecting a signal of a tracer at a certain time into the reactor and measuring its output concentration at different times. This analysis shows the time that each fluid element remains inside the reactor [4]. Three types of curves are used. The **E** curve represents the theoretical residence time distribution of the different fluid elements and is normalised according to Eq. (1); $\mathbf{E}\,\mathrm{d}t$ is the fraction of fluid whose residence time is between t and $t + \mathrm{d}t$:

$$\int_0^\infty \mathbf{E}\,\mathrm{d}t = 1 \tag{1}$$

The **C** curve represents the experimental normalised concentration distribution (similarly to Eq. (1)) of the tracer at the outlet and the **F** curve represents the accumulated tracer concentration at the reactor outlet at time t, $\mathbf{F} = \int_0^t \mathbf{C}\,\mathrm{d}t$. Two characteristics

* Corresponding author. Tel.: +44 20 7679 3832; fax: +44 20 7383 2348.
E-mail address: p.angeli@ucl.ac.uk (P. Angeli).

1385-8947/$ – see front matter © 2007 Published by Elsevier B.V.
doi:10.1016/j.cej.2007.07.021

Nomenclature

A	cross-section area of the fluid paths
c	concentration (kg/m^3)
C	concentration curve
D	hydraulic diameter
E	channel depth (m)
E	**E** curve or residence time distribution curve
F	force vector (N)
FD	divergence parameter (%)
H	phase height and characteristic length (m)
I	injection positions at the inlet, $i = 1, \ldots, I$
I_{arrived}	initial positions from which released particles reach the collecting channel
I_z	injection positions in the z plane
$I_{\perp z}$	injection positions in a plane perpendicular to the z plane
L	channel or fluid path length (m)
m	system mass (kg)
n_i	number of particles released at position i
N	total number of fluid paths
$N_{\text{Particles}}$	total number of particles released at the inlet
P	pressure (Pa)
Q	total flowrate between parallel sheets in the x direction (m^3/s)
R	fluid resistance (Pa s/m^3)
Re	Reynolds number, $\rho H v_0/\mu$
s	position where slowest particles at the inlet boundary are released
S	spread parameter
t	residence time (s)
v_{N}	normal velocity component to the inlet plane
v_x	velocity in the x direction (similar for components y and z)
v_0	characteristic velocity and mean velocity at the reactor inlet, $Q/(\pi r^2)$ (m/s)
W	channel/path width
x, y and z	spatial co-ordinates (m)
l	fluid path length or distance travelled by particle (m)
V	reactor volume
r	reactor inlet radius

Greek letters

$\delta_{i,j}$	Kronecher delta
λ_{NC}	Non-circularity coefficient for pressure drop
μ	fluid viscosity (Pa s)
ρ	fluid density (kg/m^3)
σ	standard deviation of the RTD
τ	space time defined as volume/flowrate = V/Q
ω	fluid path angle

Subscripts

A	distributing channel
B	collecting channel
EQ	equipartition
mean	mean or average
N	normal or perpendicular
P	particle
R	reaction channel/path
s	position of the slowest particle at the injection point
f	final
T	total

Superscript

#	dimensionless variable

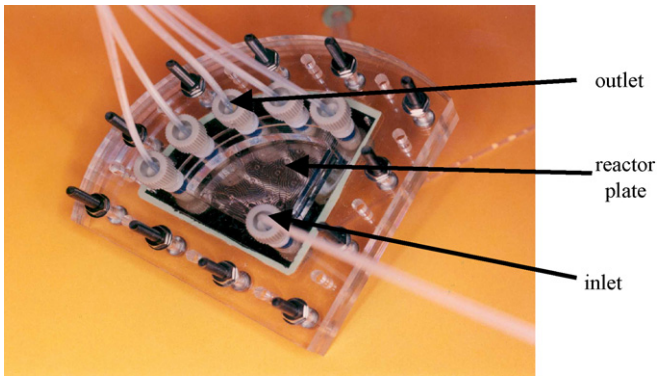

Fig. 1. Mesh microreactor prototype.

of the theoretical RTD, **E** curve, are the mean residence time, t_{E}, defined by Eq. (2) and the spread or variance of the distribution (σ_{E}^2) defined by Eq. (3). Similar equations can be written for the **C** curve. In the case of close systems or recipients (systems without tracer dispersion at the inlet/outlet boundaries [5]) and systems where the diffusion flux of the tracer is negligible when compared to the convective flux, **C** = **E** and d**F**/dt = **E**. Thus, the reactor space time for a constant density fluid is also equal to the mean time of the **C** curve, $\tau = V/Q = t_{\text{E}} = t_{\text{C}}$:

$$t_{\text{E}} = \tau = \int_0^\infty t\mathbf{E}\,\mathrm{d}t \quad \text{or} \quad t_{\text{E}} = \tau \cong \sum_{i=0}^{i=N} t_i \mathbf{E}_i \Delta t_i$$

(for N discrete values) (2)

$$\sigma_{\text{E}}^2 = \int_0^\infty t^2\mathbf{E}\,\mathrm{d}t - t_{\text{E}}^2 \quad \text{or} \quad \sigma_{\text{E}}^2 \cong \sum_{i=0}^{i=N} t_i^2 \mathbf{E}_i \Delta t_i - t_{\text{E}}^2$$

(for N discrete values) (3)

2. Theoretical analysis of residence time distribution in the mesh microreactor

The mesh microreactor (see Fig. 2a for a schematic diagram) features a nickel mesh with a non-active region of 5.6 mm length and 30 μm thickness and an active region (with microfabricated pore openings) of 26.4 mm length and 5 μm thickness. The phase

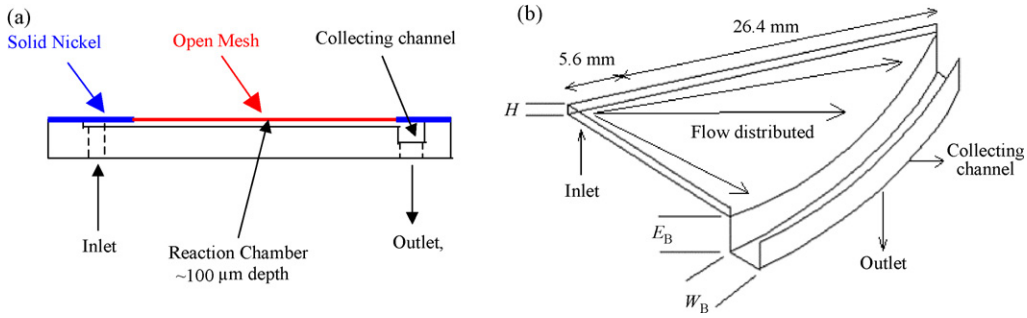

Fig. 2. Diagram of the bottom half of the mesh microreactor: (a) side view of fluidic chamber and reactor case; (b) 3D view of the bottom half fluidic chamber, which includes a collecting channel.

height above and below the mesh is 100 μm. A collecting channel is placed at the back of the mesh after the active region. The standard plate geometry is a simple 90° quadrant with a fixed distance of 32 mm from the inlet to the collecting channel [6]. Fig. 2 shows the bottom part of the mesh microreactor where one phase flows. The top part is simply a mirror image of the one shown in the figure and both of them are separated by the mesh and clamped together.

The initial dimensions of the collecting channel are $W_B = 3000\ \mu m$ and $E_B = 1000\ \mu m$ (see Fig. 2b). All the fluid in the collecting channel leaves through a single 1 mm bore hole located in the middle. It was found that multiple outlets along the collecting channel were impractical, except during the priming stage, due to difficulties in balancing the flows in the outlet tubes.

Dimensionless variables are defined using the phase height over the reactor plate H as the characteristic length, the inlet velocity to the reactor v_0 as the characteristic velocity and a characteristic pressure based on viscosity, $\mu v_0/H$ (see Eqs. (4)–(7)). The characteristic pressure is suitable for systems with low Reynolds numbers (range of interest in microreactors) where viscous effects are dominant over inertial effects [7]:

$$x^{\#} = \frac{x}{H}, \quad E^{\#} = \frac{E}{H}, \quad W^{\#} = \frac{W}{H}, \quad L^{\#} = \frac{L}{H}, \quad A^{\#} = \frac{A}{H^2} \tag{4}$$

$$v^{\#} = \frac{v}{v_0}, \quad Q^{\#} = \frac{Q}{v_0 H^2} \tag{5}$$

$$t^{\#} = \frac{t v_0}{H} \tag{6}$$

$$P^{\#} = \frac{P}{\mu v_0/H} \tag{7}$$

2.1. Simplified resistance network model

A simplified methodology based on the analogy between viscous flow and electrical resistance networks is used to analyse flow distribution in the mesh microreactor. The general methodology is described in detail in [3]. The resistance network model (RNM) for a consecutive manifold [3] is applied to the current geometry considering the following assumptions: (a) straight streamlines along the reaction plate (this assumption will be checked later via computational fluid dynamics modelling, CFD), (b) 2D flow in the reaction plate, which is justified as the phase height is substantially smaller than the other two dimensions.

Fig. 3 shows a top view of the reaction plate in the mesh microreactor (dashed lines represent a modified geometry discussed later). This system is equivalent to the consecutive structure given in Fig. 4, with the difference that the resistances along the distributing channel are zero ($R_{A,i} = 0$, common inlet port). Eqs. (8) and (9) define the linear system of equations for the flow in the N discretised reactor fluid paths. Only half the reaction plate is considered (from side wall to centreline of reaction plate) in both the RNM and CFD analyses since the flow in the other side is symmetrical:

$$-\sum_{k=j+1}^{k=N} Q^{\#}_{R,k} \frac{R^{\#}_{A,(j+1)}}{R^{\#}_{R,j}} + \sum_{k=1}^{k=j} Q^{\#}_{R,k} \frac{R^{\#}_{B,(N-j+1)}}{R^{\#}_{R,j}} - Q^{\#}_{R,(j+1)} \times \frac{R^{\#}_{R,(j+1)}}{R^{\#}_{R,j}} + Q^{\#}_{R,j} = 0, \quad j = 1, 2, \ldots, (N-1) \tag{8}$$

$$\sum_{k=1}^{k=N} Q^{\#}_{R,k} = Q^{\#}_{T} \tag{9}$$

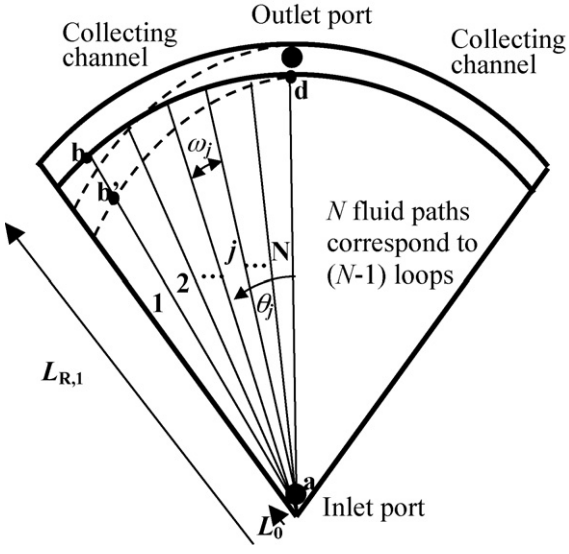

Fig. 3. Top view of the reaction plate with N discretised fluid paths in half the geometry for application of the resistance network model.

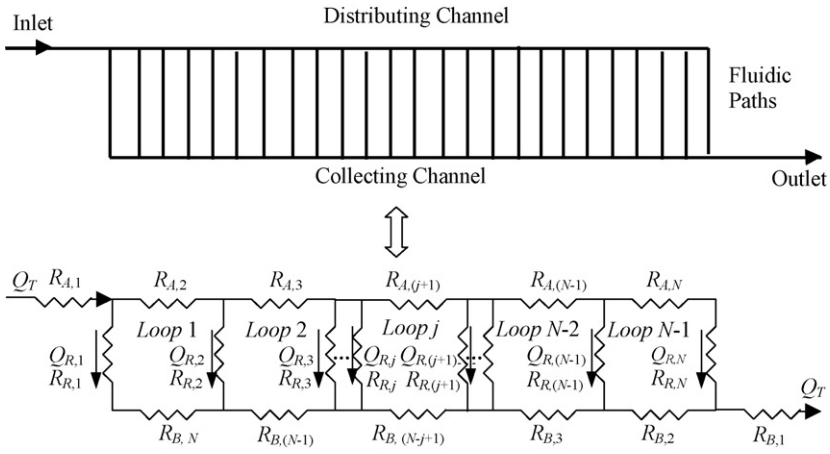

Fig. 4. Resistance network for consecutive structure according to [3].

2.2. Available designs for even residence time distribution

Two different design approaches are considered below to achieve even flow and/or residence time distribution in the reaction plate.

2.2.1. Reaction plate with quadrant shape (constant distance between inlet port and collecting channel)

Because of the reactor shape, even flow distribution in the different fluid paths also ensures the same mean residence time in each fluid path. Considering the close loop defined by paths a–b, b–d and a–d in Fig. 3, a pressure drop balance results in Eq. (10). In order to have equal flow along paths a–b and a–d, $\Delta P_{\text{b–d}}$ should be equal to 0, which means that the pressure drop across the collecting channel should be negligible.

$$\Delta P_{\text{a–b}} + \Delta P_{\text{b–d}} = \Delta P_{\text{a–d}} \tag{10}$$

The pressure drop along the fluid paths that go from the inlet port to the collecting channel is calculated via Eq. (11), which assumes 2D flow between parallel sheets [8]:

$$\frac{\partial P^{\#}}{\partial x^{\#}} = -\frac{12}{W^{\#}} Q^{\#} \tag{11}$$

The change in the path width along the discretised fluid paths implies a change in the velocity, which needs to be integrated along the path length in order to get the total pressure drop. For a quadrant-type structure, the path width is a function of the distance from the port inlet l and the angle of the fluid path ω, $W^{\#}(l) = \omega(\text{rad}) l^{\#}$. Integration of Eq. (11) along each fluid path i, from $l^{\#} = L_0^{\#}$ (the non-active length immediately after the inlet) to $l^{\#} = L_{\text{R},i}^{\#}$ yields Eq. (12):

$$\Delta P_{\text{R},i}^{\#} = 12 Q_{\text{R},i}^{\#} \int_{L_0}^{L_{\text{R},i}} \frac{1}{W^{\#}(l^{\#})}\, \mathrm{d}l^{\#} = \frac{12 Q_{\text{R},i}^{\#}}{\omega(\text{rad})} (\ln(L_{\text{R},i}^{\#}) - \ln(L_0^{\#})) \tag{12}$$

where the subscript "R,i" indicates flow path i in the reaction plate. The pressure drop along each path i is also expressed as $\Delta P_{\text{R},i}^{\#} = R_{\text{R},i}^{\#} Q_{\text{R},i}^{\#}$ where the resistance $R_{\text{R},i}^{\#}$ is given by Eq. (13):

$$R_{\text{R},i}^{\#} = \frac{12(\ln(L_{\text{R},i}^{\#}) - \ln(L_0^{\#}))}{\omega(\text{rad})} \tag{13}$$

The resistance in the collecting channel for calculating pressure drop as $\Delta P_{\text{B},i}^{\#} = R_{\text{B},i}^{\#} Q_{\text{B},i}^{\#}$ is obtained from Eq. (14) [3], where $D^{\#}$ is the dimensionless hydraulic diameter defined by $D^{\#} = 4E^{\#}W^{\#}/(2E^{\#} + 2W^{\#})$ for a rectangular channel:

$$R_{\text{B},i}^{\#} = \frac{128 L_{\text{B},i}^{\#} \lambda_{\text{NC,B},i}}{D_{\text{B},i}^{\#4} (E_{\text{B},i}^{\#}/W_{\text{B},i}^{\#} + W_{B,i}^{\#}/E_{\text{B},i}^{\#} + 2)} \tag{14}$$

2.2.2. Modified plate geometry

2.2.2.1. Plate geometry for flow equipartition. The previous approach would generally require large collecting channels to achieve flow equipartition by making pressure drop along the collecting channel negligible. Large collecting channel volume though increases the sample dispersion. Even flow distribution can be achieved by modifying the quadrant shape of the reaction plate as shown in Fig. 3 (dashed lines define new collecting channel). Thus, a–b′ < a–d and path a–b′ can have the same flowrate as path a–d but with reduced pressure drop (shorter path). The resistance network model yields a simplified solution when equal flowrates $Q_{\text{R},i}^{\#}$ within each discretised fluid path are considered in conjunction with $R_{\text{A},(j+1)}^{\#} = 0$. In this case, the system of N equations defined by Eqs. (8) and (9) reduces to the following $(N-1)$ independent equations:

$$j R_{\text{B},(N-j+1)}^{\#} - R_{\text{R},(j+1)}^{\#} + R_{\text{R},j}^{\#} = 0, \quad j = 1, \ldots, (N-1) \tag{15}$$

Substituting the values of resistances $R_{\text{B}}^{\#}$ and $R_{\text{R}}^{\#}$ in Eq. (15), Eq. (16) is obtained:

$$\frac{32 j \lambda_{\text{NC},(N-j+1)} (E_{\text{B},(N-j+1)}^{\#} + W_{\text{B},(N-j+1)}^{\#})^2 L_{\text{B},(N-j+1)}^{\#}}{4 E_{\text{B},(N-j+1)}^{\#3} W_{\text{B},(N-j+1)}^{\#3}} - \frac{12(\ln(L_{\text{R},(j+1)}^{\#}) - \ln(L_{\text{R},j}^{\#}))}{\omega} = 0, \quad j = 1, \ldots, (N-1) \tag{16}$$

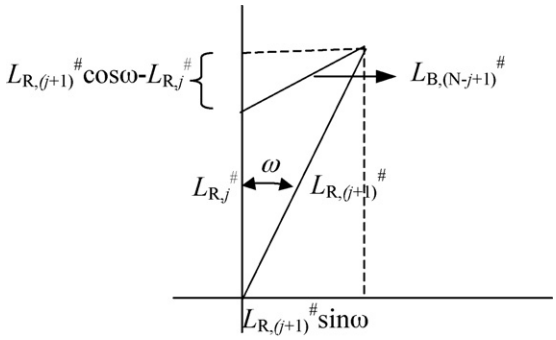

Fig. 5. Calculation of the collecting channel path lengths $L_{B,(N-j+1)}$.

where $L^{\#}_{B,(N-j+1)}$ is a function of the unknown path length $L^{\#}_{R,j}$ given by Eq. (17) when a straight collecting sub-path is assumed (see Fig. 5 where lines join the centres of the fluid paths):

$$L^{\#}_{B,(N-j+1)} = \sqrt{\left(L^{\#}_{R,(j+1)} \sin\omega\right)^2 + \left(L^{\#}_{R,(j+1)} \cos\omega - L^{\#}_{R,j}\right)^2} \tag{17}$$

Eq. (16) represents $N-1$ equations that can be solved independently since the value of $L^{\#}_{R,N}$ is known (path length in the middle of the reactor). A non-linear root finder method is used (bisection/secant methods) in order to solve the non-linear term $L_{R,j}$ by using $L^{\#}_{R,(j+1)}$ as an initial guess. Therefore, the second value calculated for $j=N-1$ is $L^{\#}_{R,j} = L^{\#}_{R,(N-1)}$ and the process is repeated up to $L^{\#}_{R,1}$. A large N value (many fluid paths) is used for better accuracy.

While this approach ensures that the flowrates in the discretised fluid paths are the same, different path lengths result in different residence times from inlet to collecting channel. A mesh with quadrant geometry (active region of the plate) should, therefore, be adopted in order to ensure that the mean residence times in all fluid paths in the active mesh region are the same. This, however, implies that a large area of the plate is non-active, which results in unnecessary additional dispersion (see Fig. 6). With this approach the size of the collecting channel, and the dispersion in it, is reduced to the expense of increased dispersion in the non-active area of the plate.

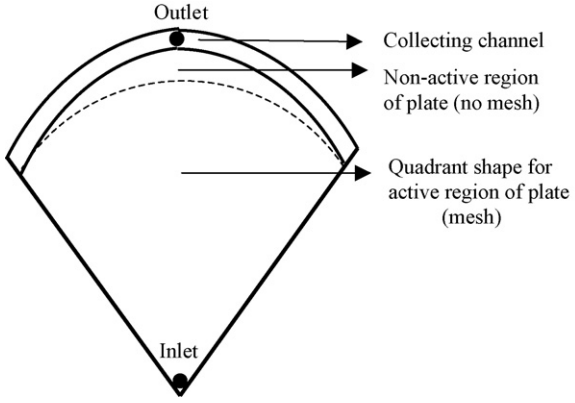

Fig. 6. Modified plate geometry for flow equipartition.

2.2.2.2. Plate geometry for equal mean residence times in fluid paths. A better approach is to design the reaction plate so that all fluid paths have the same mean residence time defined by Eq. (18):

$$t^{\#}_{R,i} = \frac{L^{\#}_{R,i} - L^{\#}_{0}}{Q^{\#}_{R,i}/A^{\#}_{R,i}} \tag{18}$$

An average fluid path area is obtained by integrating the perpendicular area to the flow $H\omega l$ along the fluid path length $(L^{\#}_{R,i} - L^{\#}_{0})$:

$$A^{\#}_{R,i} = \frac{\int_{L^{\#}_0}^{L^{\#}_{R,i}} \omega l^{\#}\, \mathrm{d}l^{\#}}{L^{\#}_{R,i} - L^{\#}_{0}} = \frac{\omega(L^{\#2}_{R,i} - L^{\#2}_{0})}{2(L^{\#}_{R,i} - L^{\#}_{0})} = \frac{\omega(L^{\#}_{R,i} + L^{\#}_{0})}{2} \tag{19}$$

The optimised geometry for the same mean residence time in all fluid paths is found via an iterative procedure. Given a desired mean residence time, $t^{\#}_{R,i} = t^{\#}_{\mathrm{desired}}$ the required initial quadrant radius is obtained from Eq. (20):

$$L^{\#}_{R,i} = L^{\#}_{0} + \frac{t^{\#}_{R,i} Q^{\#}_{R,i}}{A^{\#}_{R,i}} \tag{20}$$

where $A^{\#}_{R,i}$ is given by Eq. (19) and flowrates are calculated assuming the same flowrate in all fluid paths; for the first iteration $Q^{\#}_{R,i} = Q^{\#}_{EQ}$ (flow equipartition flowrate $Q^{\#}_{EQ}$). New flowrates $Q^{\#}_{R,i}$ along each fluid path in this initial quadrant shape are found from Eqs. (8) and (9) as previously shown. The calculated flowrates $Q^{\#}_{R,i}$ are used to recalculate the fluid path lengths that produce the same desired residence time via Eq. (20), which results in a new plate geometry. This process is repeated until the new calculated flowrates are within an acceptable tolerance of the previous values.

2.3. Particle tracking

A robust approach to obtain residence time distributions is to solve the steady-state flow field inside the reactor via CFD and conduct Lagrangian particle tracking with weightless particles that follow the flow streamlines. This overcomes the numerical diffusion issue generally found when solving the convection-diffusion equation at high Peclet numbers [9]. A statistically large number of particles are released at the inlet of the reactor (boundary conditions for particle i, $p_{0,i} = (x_{0,i}, y_{0,i}, z_{0,i})$) and the position of each particle at time $t^{\#}$ is obtained from

$$v^{\#}_{z}(x^{\#}, y^{\#}, z^{\#}) = \frac{\mathrm{d}x^{\#}}{\mathrm{d}t^{\#}}, \qquad v^{\#}_{y}(x^{\#}, y^{\#}, z^{\#}) = \frac{\mathrm{d}y^{\#}}{\mathrm{d}t^{\#}},$$
$$v^{\#}_{z}(x^{\#}, y^{\#}, z^{\#}) = \frac{\mathrm{d}z^{\#}}{\mathrm{d}t^{\#}} \tag{21}$$

A finite element software (FEMLAB 3.0) was used to obtain the flow field in different mesh microreactor geometries by solving the dimensionless Navier–Stokes and continuity equations (see dimensionless numbers' definitions in Eqs. (4)–(7)). Single-phase flow is solved in half of the reaction plate (see Fig. 7). All geometries analysed feature a collecting channel of width

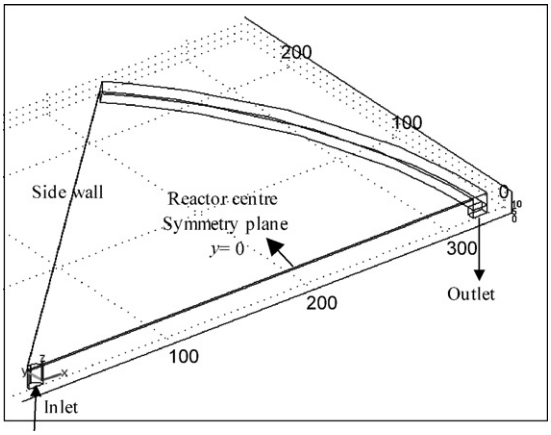

Fig. 7. Half the geometry of a standard quadrant mesh microreactor. The characteristic dimension is the phase height, $H^{\#} = 1$.

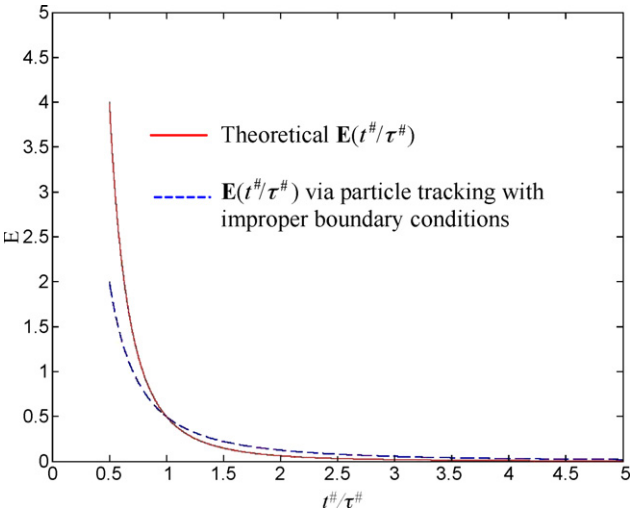

Fig. 8. Comparison between the theoretical **E** curve and that obtained via particle tracking using a finite set of particles distributed uniformly at the inlet during laminar flow in a circular pipe.

$W_B^{\#} = 10$. Splines are used to interpolate the collecting channel curve, converted into a 2D geometry and imported into FEMLAB. Since the geometry features a large aspect ratio of length ($L^{\#} = 330$) to phase height ($H^{\#} = 1$), the number of tetrahedral elements is reduced by scaling the geometry in the z direction by a factor between 5 and 10 to produce *non-isotropic* second-order Lagrange p2–p1 elements. Meshing functions are used to limit the element size along certain edges and faces. The resulting anisotropic mesh contains between 15,000 and 22,000 elements in all cases.

The Hagen Poiseuille parabolic velocity profile, $v_z^{\#} = 2v_0^{\#}(1 - ((x^{\#} - x_{\text{centre}}^{\#})^2 + (y^{\#} - y_{\text{centre}}^{\#})^2)/r^{\#2})$ is used as boundary condition in the inlet channel of radius $r^{\#} = 5$. The characteristic velocity is the average inlet velocity $v_0 = Q_T/(\pi r^2)$. The solver GMRES is utilised with incomplete LU preconditioning, non-linear tolerance of 1E−7 and drop tolerance = 0.0007.

Particle tracking quality depends upon the quality of the velocity field solution and the time step used to solve the system of equations given in Eq. (21). Calculation of the RTD via particle tracking requires special consideration of the boundary condition for the particle release when the velocity profile at the inlet is not flat. When the injection consists of a finite number of particles uniformly distributed at the inlet, the calculated RTD is incorrect as Fig. 8 shows for laminar flow in a pipe where the theoretical **E** curve is given by Fogler [5] as $\mathbf{E}(t^{\#}/\tau^{\#}) = 1/(2(t^{\#}/\tau^{\#})^3)$.

Different approaches where either the residence time is calculated based on particle volume flux weighting or an initial distribution of point co-ordinates with respect to a momentum or velocity weighting is used have been discussed by Johnson [10] and Zitny [11]. The approach simulates the release of a *fixed concentration of particles in a finite time* (as in a tracer injection). I particle injection points are uniformly distributed. More fluid elements and therefore released particles cross the inlet boundary in a differential of time at positions of high velocities as shown in Fig. 9.

The distance travelled by particle i in a differential of time $\mathrm{d}t^{\#}$ is $\mathrm{d}l_i^{\#} = v_{\mathrm{N},i}^{\#}\,\mathrm{d}t^{\#}$ and Eq. (22) applies where $v_{\mathrm{N},i}^{\#}$ is the dimensionless perpendicular velocity component to the inlet plane. Particles released at position $i = s$ are the slowest ones (vicinity of the wall, $s = 1$ in Fig. 9):

$$\frac{\mathrm{d}l_1^{\#}}{v_{\mathrm{N},1}^{\#}} = \frac{\mathrm{d}l_2^{\#}}{v_{\mathrm{N},2}^{\#}} = \cdots = \frac{\mathrm{d}l_i^{\#}}{v_{\mathrm{N},i}^{\#}} = \cdots = \frac{\mathrm{d}l_{I-1}^{\#}}{v_{\mathrm{N},I-1}^{\#}} = \frac{\mathrm{d}l_I^{\#}}{v_{\mathrm{N},I}^{\#}} = \mathrm{d}t^{\#} \tag{22}$$

The time interval $\mathrm{d}t^{\#}$ is chosen so that the distance walked by the slowest particle is equivalent to its diameter $d_P^{\#}$, $\mathrm{d}l_s^{\#} = d_P^{\#}$. The number of particles released at position i is n_i and it is normalised so that $n_s = 1$ and n_i is obtained via Eq. (23):

$$n_i = \frac{\mathrm{d}l_i^{\#}}{\mathrm{d}l_s^{\#}} = \frac{v_{\mathrm{N},i}^{\#}}{v_{\mathrm{N},s}^{\#}} \tag{23}$$

According to this approach, the total number of particles released is given by $N_{\text{Particles}} = \sum_{i=1}^{n=I} n_i$. Thus, considering I injection points with n_i particles per injection point ($i = 1, \ldots, I$), the $\mathbf{E}(t^{\#}/\tau^{\#})$ curve coincides exactly with the theoretical curve in the example shown in Fig. 8.

The system of equations given by Eq. (21) is solved via a second-order Runge–Kutta scheme. Particles are released at the beginning of the active region (5.6 mm from the inlet port, $R^{\#} = 56$) at different z planes. In each z plane, particles are uniformly distributed along an arc at I_z positions and the total number of initial positions is $I = \sum I_z$. The x and y co-ordinates are given by $x_i^{\#} = R^{\#}\cos(\theta(i-1))$ and $y_i^{\#} = R^{\#}\sin(\theta(i-1))$, where i is the position number in the z plane considered.

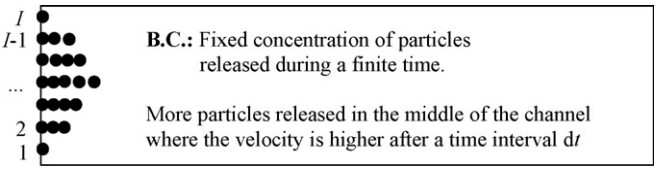

Fig. 9. Proper boundary condition for particle injection at the reactor inlet in order to calculate the residence time distribution.

When conducting particle tracking the **E** curve can be obtained by Eq. (24), where p_i is the number of particles with a residence time $t_i^\# < t^\# < t_i^\# + \Delta t_i^\#$, $p_i = \sum n_k = \sum(v_{N,k}^\# / v_{N,s}^\#)$ where k refers to those positions from which the released particles have a residence time within $t_i^\#$ and $t_i^\# + \Delta t_i^\#$. $N_{Particles}$ is the total number of particles released, $N_{Particles} = \sum n_i$. This definition ensures that **E** satisfies Eq. (1).

$$\mathbf{E}_i\left(\frac{t^\#}{\tau^\#}\right) = \frac{p_i}{(\Delta t_i^\#/\tau^\#)N_{Particles}} \tag{24}$$

3. Results and discussion

3.1. Flow and residence time distribution via the resistance network model

3.1.1. Reaction plate with quadrant shape

Fig. 10 shows the flow distribution along 200 discretised fluid paths in half the reaction plate of a mesh microreactor with standard quadrant geometry calculated via the resistance network model (see Section 2.1). The collecting channel has a width of $W_B^\# = 10$ and different depths from $E_B^\# = 1$ to 7. In all cases, flowrates at the centre of the reactor are higher than those found at the side of the reactor.

A divergence parameter FD (*flow distribution*) defined by Eq. (25) in which $Q_{R,i}$ is the flowrate within each fluid path is calculated for each collecting channel size: 0.7% ($E_B^\# = 7$), 2.2% ($E_B^\# = 4$), 3.9% ($E_B^\# = 3$), 8.5% ($E_B^\# = 2$) and 25.6% ($E_B^\# = 1$). For $E_B^\# < 3$ the flow distribution along the reaction plate becomes substantially uneven with flowrates along the fluid paths deviating from the equipartition flowrates by more than 3.9%.

$$\mathrm{FD}\,(\%) = \max_{j=1}^{N}\left[100\frac{|Q_{EQ}^\# - Q_{R,j}^\#|}{Q_{EQ}^\#}\right] \tag{25}$$

3.1.2. Modified plate geometry

Flow equipartition along the fluid paths of the active mesh region can also be achieved by modifying the simple quadrant shape geometry. This approach allows the collection channel depth to be small (less than 700 μm) thus reducing tracer dispersion in it. As discussed in Section 2.2, this can be done in two ways:

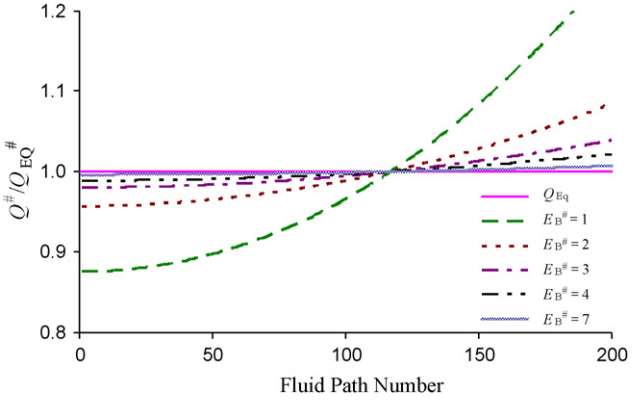

Fig. 10. Flow distribution in 200 discretised fluid paths in half of the reaction plate (from side wall, 0, to reactor centre, 200) of the mesh microreactor with standard quadrant geometry obtained via the resistance network model.

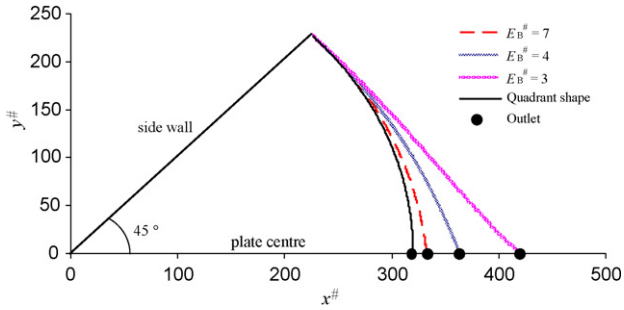

Fig. 11. Half plate geometries (from reactor centre to side wall) for flow equipartition as a function of collecting channel depth, $E_B^\#$, for a collecting channel width of $W_B^\# = 10$.

3.1.2.1. Plate geometry for flow equipartition. Fig. 11 shows half plate geometries that produce identical flowrates in all discretised fluid paths calculated via Eq. (16) as a function of the collecting channel depth $E_B^\#$ and a constant width of $W_B^\# = 10$. The other half of the reaction plate is symmetrical. Since the flowrates are the same in all paths but their lengths are different the mean residence times will also be different. This is resolved by having an active plate region with mesh that has pores with quadrant shape. However, although the collecting channel volume can be reduced, there is an extra non-active volume between the quadrant shape of the active plate region and the collecting channel that causes extra overall dispersion (see Fig. 6).

3.1.2.2. Plate geometry for equal mean residence times in fluid paths. Half plate designs for the same residence time in all fluid paths are shown in Fig. 12. In this case, large reductions in the collecting channel depth cause small changes in the reaction plate geometry. Furthermore, the whole reactor plate is active (mesh with pores in the whole area) so that no dispersion occurs in it.

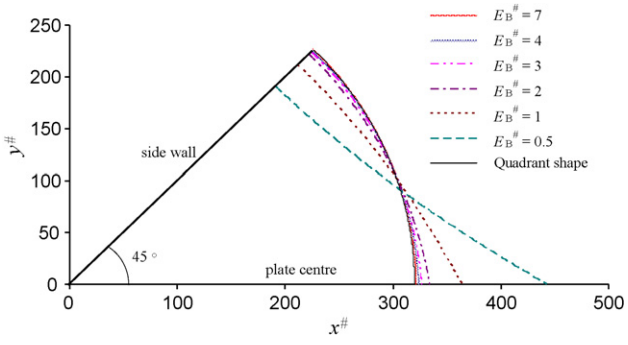

Fig. 12. Half plate geometries (from reactor centre to side wall) for identical mean residence time in all fluid paths as a function of collecting channel depth $E_B^\#$, for a collecting channel width of $W_B^\# = 10$.

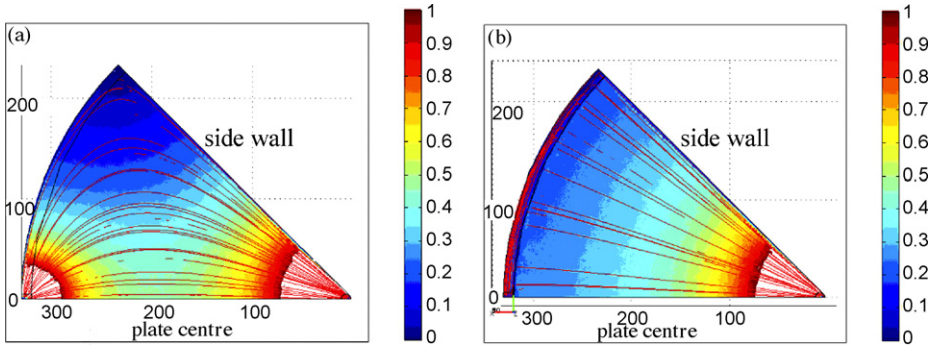

Fig. 13. Dimensionless velocity field and streamlines at the middle plane of half reaction plate with quadrant shape geometry when $Re = 1.061$ for (a) no collecting channel; (b) collecting channel of depth $E_B^{\#} = 7$ and width $W_B^{\#} = 10$.

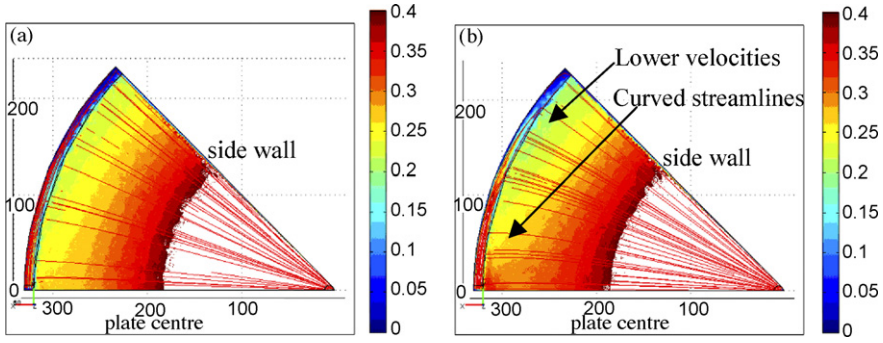

Fig. 14. Dimensionless velocity field and streamlines at the middle plane of half reaction plate with quadrant shape geometry when $Re = 1.061$ for (a) collecting channel of depth $E_B^{\#} = 7$; (b) collecting channel of depth $E_B^{\#} = 4$. Collecting channel width $W_B^{\#} = 10$.

3.2. Flow and residence time distribution via numerical simulations and particle tracking

3.2.1. Velocity field on the reactor plate

The same geometries as those analysed in Section 3.1 are also studied with FEMLAB to obtain the flow field on the reaction plate. All models are for $Re = \rho v_0 H/\mu = 1.061$ that corresponds to a water system at $Q = 500\,\mu$l/min. The dimensionless mean residence time in the reaction plate (volume = 7.9818×10^{-8} m^3/s) is $t_{mean}^{\#} = 1016.3$.

Figs. 13 and 14 show the flow field and streamlines at the middle z plane in half of the reaction plate of standard quadrant shape, for three different collecting channel depths, namely, $E_B^{\#} = 0$, $E_B^{\#} = 7$, and $E_B^{\#} = 7$, $E_B^{\#} = 4$, respectively. It can be seen that as the collecting channel depth increases the streamlines become straighter, which means that the flow distributes more evenly across the plate. This agrees with findings from the resistance network model where FD = 0.7% for $E_B^{\#} = 7$, while FD = 2.2% for $E_B^{\#} = 4$. The microreactor with a collecting channel depth $E_B^{\#} = 7$ produces even flow.

Applying the resistance network model, a new plate geometry for flow equipartition in all fluid paths (FD = 0%) was obtained for $E_B^{\#} = 4$ as shown in Fig. 15 (see also Fig. 11). It can be seen that indeed this geometry yields even flow distribution (identical velocities for same radial positions as shown by the dashed line in Fig. 15) compared to that in Fig. 14b for the standard quadrant shape geometry with the same collecting channel depth.

To minimise the non-active volume in the plate, the plate geometry was modified using the resistance network model (Section 3.1) for even mean residence time in all discretised fluid paths as shown in Fig. 12. A depth of $E_B^{\#} = 1$ is chosen to substantially reduce dispersion in the collecting channel and reactor flushing time. In this case the flow is not equally

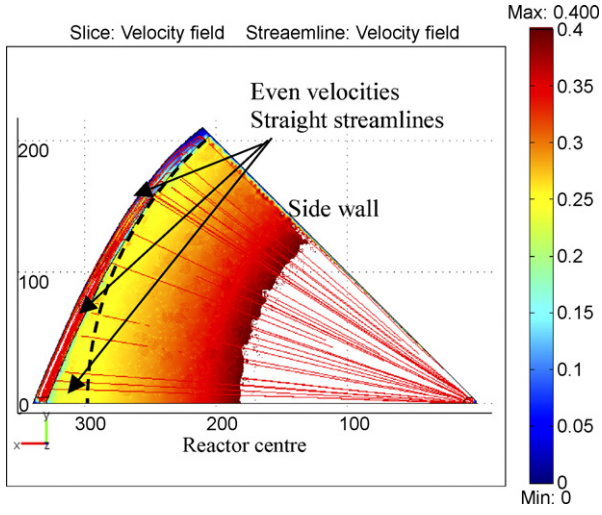

Fig. 15. Dimensionless velocity field at the middle plane of half of the reaction plate with a modified plate geometry obtained via the resistance network model (see Fig. 11) when $Re = 1.061$ and the collecting channel has $E_B^{\#} = 4$ and $W_B^{\#} = 10$.

Table 1
Particle tracking parameters for the different reactor plate geometries analysed

	Quadrant geometry				Modified geometry
	$E_B^\# = 7$	$E_B^\# = 4$	$E_B^\# = 1$	$E_B^\# = 0$	$E_B^\# = 1$ (Fig. 12)
$I_{arrived}$ [a]	1271	1751	1733	1421	1825
$t^\#_{mean}/\tau^\#$	0.6357	0.5983	0.457	0.3975	0.551
$N_{Particles}$	194210	207420	196820	131350	136360
$N_{arrived}$	96524	123330	121800	71119	93715

[a] $I_{arrived}$ indicates the number of injection locations from which released particles arrived to the collecting channel.

distributed among the different fluid paths (streamlines are not straight) and no quantitative comparison between the standard and the modified geometries can be made based on the velocity field. Particle tracking will be used to obtain RTD curves in the modified geometries.

3.2.2. Residence time distributions via Lagrangian particle tracking

Weightless particle tracking is conducted to obtain the RTD on the reaction plate according to the method described in Section 2.3. Due to the large aspect ratio of the plate, a very small time step is required for accurate particle tracking. As indicated above, $t^\#_{mean} = 1016.3$ and $Re = 1.061$ are used for all geometries. Particle tracking is conducted in 5 different geometries using $I_z = 200$, $I_{\perp z} = 15$, $I = 3000$, $\Delta t^\# = 2$ and final time $t^\#_f = 3500$ (1751 time steps). Particles are stopped as soon as they enter the collecting channel. Table 1 shows the initial and boundary conditions utilised for particle tracking in all geometries.

Fig. 16 shows normalised **E** curves for a quadrant shape mesh microreactor with different collecting channel depths $E_B^\#$. As the collecting channel depth increases the spread of the RTD decreases and the RTD becomes more similar to that for 2D laminar flow. Table 1 shows that a substantial amount of released particles do not reach the collecting channel or are not resolved during the simulated time $t^\#_f = 3500$. Due to memory problems, it is not possible to increase $t^\#_f$ and reduce the time step in order to resolve more particles. Therefore, in order to compare them,

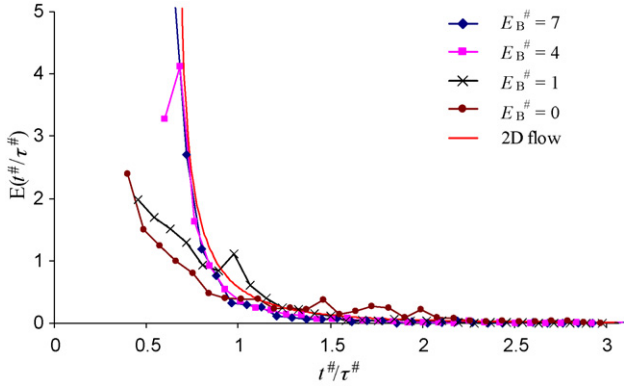

Fig. 16. Normalised RTD curves for a quadrant shape mesh microreactor for different collecting channel depths, $E_B^\#$, compared to the theoretical curve for 2D laminar flow.

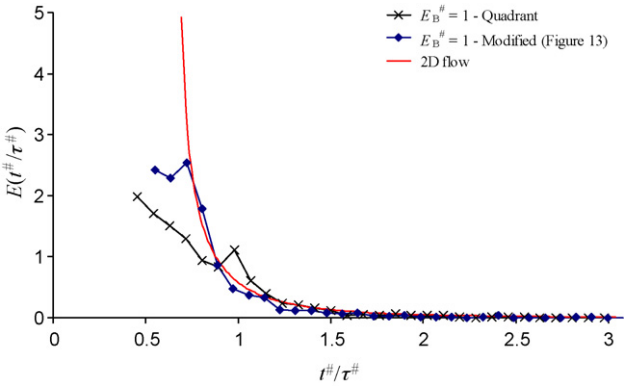

Fig. 17. Normalised RTD curves for standard quadrant and modified (see Fig. 12) reactor plate geometries with collecting channel depth $E_B^\# = 1$. Results are compared to the theoretical curve for 2D laminar flow.

the different **E** curves have been normalised using the number of particles that arrived, $N_{arrived}$ (55–69% of the released ones).

Fig. 17 shows RTDs for two plate geometries with the same collecting channel depth $E_B^\# = 1$; one is the standard quadrant geometry and the other is a modified one based on the RNM for the same mean residence time in all fluid paths (see Fig. 12 for $E_B^\# = 1$). The modified geometry shows a smaller RTD spread than the quadrant geometry although it does not result in identical mean residence times in all fluid paths (compare to solution for $E_B = 700$ μm in Fig. 16). This is because the assumption of straight streamlines in the resistance network model does not hold entirely (slightly curved streamlines).

The dimensionless mean residence times obtained from the RTDs shown in Figs. 16 and 17 via Eq. (2) are slightly smaller than 1 since the particle tracking is only simulated up to $t^\# = 3500$ ($\tau^\# = 1016.3$ in all cases). In order to characterise the spread of the distributions, a spread parameter defined by $S = \sigma_E/t_{mean}$ (%) is calculated for all distributions as shown in Table 2. The spread of the RTD for a collecting channel depth of $E_B^\# = 1$ is considerably improved when the modified reaction plate geometry shown in Fig. 12 ($S = 35.8\%$) is used, compared to the quadrant shape ($S = 42.6\%$).

4. Experimental results

The flow distribution in the mesh microreactor was also studied experimentally using *m*-cresol purple indicator as tracer in an aqueous 0.1 M NaOH solution at 500 and 1000 μl/min. The pur-

Table 2
Mean residence time, standard deviation and spread parameter for the residence time distribution curves obtained via particle tracking for different mesh microreactor geometries analysed

	Quadrant geometry				Modified geometry
	$E_B^\# = 7$	$E_B^\# = 4$	$E_B^\# = 1$	$E_B^\# = 0$	$E_B^\# = 1$ (Fig. 12)
$t^\#_{mean}/\tau^\#$	0.811	0.826	0.844	0.919	0.831
σ_E	0.269	0.304	0.359	0.547	0.297
$\sigma_E/(t^\#_{mean}/\tau^\#)$ (%)	33.2	36.8	42.6	59.5	35.8

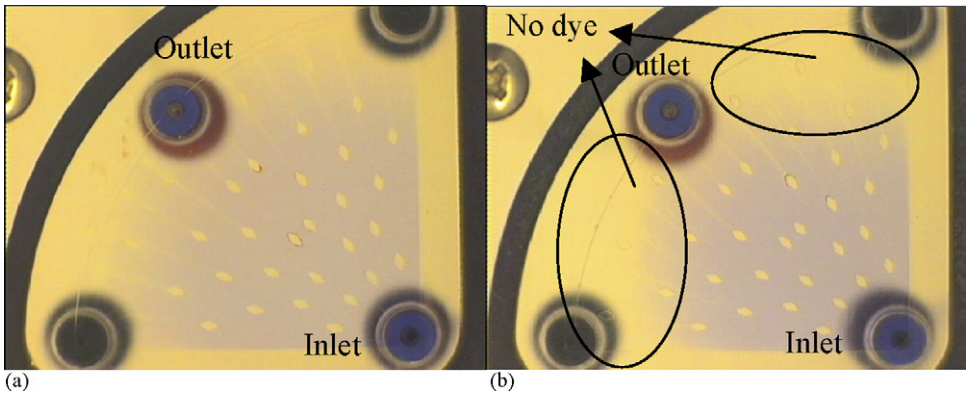

Fig. 18. Injection of 0.1 M NaOH solution with *m*-cresol dye at $Q = 0.5$ ml/min ($Re = 1.06$) into a quadrant shape mesh microreactor for collecting channel with width $W_B^{\#} = 10$ and depth (a) $E_B^{\#} = 7$ and (b) $E_B^{\#} = 4$.

pose of the experiments was to qualitatively support the main conclusions obtained from the resistance network model and CFD simulations. A tracer volume of at least 300 μl is required to ensure even concentration across the reactor for certain period of time. For the experimental studies the mesh surface and the reactor chamber were made from transparent acrylic material. It should be noted that the flow pictures below show the entire reaction plate (theoretical analyses were carried out on half of the reaction plate).

Three different geometries with a phase height of $H = 100$ μm were investigated: (a) quadrant reactor plate of radius $L^{\#} = 320$ with collecting channel of $W_B^{\#} = 10$ and $E_B^{\#} = 7$, (b) quadrant reactor plate of radius $L^{\#} = 320$ with collecting channel of $W_B^{\#} = 10$ and $E_B^{\#} = 4$ and (c) modified plate geometry for flow equipartition with collecting channel of $W_B^{\#} = 10$ and $E_B^{\#} = 4$. Fig. 18 compares dye concentration for cases (a) and (b). While the dye concentration is fairly uniform when $E_B^{\#} = 7$ (FD = 0.7% from the RNM), the geometry with $E_B^{\#} = 4$ shows smaller dye concentration away from the reactor centre than at the centre for identical radial positions (FD = 2.2% from the RNM).

Fig. 19 shows a mesh microreactor where the plate geometry has been modified to deliver even flow distribution (as theoretically presented in Fig. 15 for $E_B^{\#} = 4$). This is an intermediate geometry between those geometries presented in Fig. 11 for $E_B^{\#} = 4$ and 3. It can be seen that in this geometry the tracer front is at similar radial positions (which would indicate same flowrate in all fluid paths). Therefore, if a quadrant active plate region is implemented (dashed line in Fig. 19) the spread of the mean residence times for all fluid paths in the reaction plate will be small.

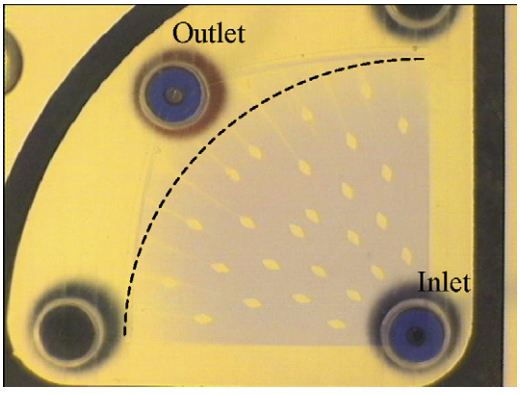

Fig. 19. Injection of 0.1 M NaOH solution with *m*-cresol dye at $Q = 0.5$ ml/min ($Re = 1.06$) in a modified reactor plate geometry for even flow distribution for collecting channel with $W_B^{\#} = 10$ and $E_B^{\#} = 4$.

5. Conclusions

An analytical methodology based on a resistance network model (RNM) is implemented to investigate flow and residence time distribution in a mesh microreactor with initial quadrant shape geometry. The results are compared with those obtained from detailed numerical simulations of the flow field using CFD and from particle tracking analysis in order to validate the RNM assumptions. Proper boundary conditions for particle release are necessary for the calculation of accurate RTD curves. The RNM is applied to quickly find geometries that yield even residence time distribution inside the reaction plate (active region) while minimising the non-active microreactor volume. Small non-active reactor volumes are important for reducing microreactor emptying/flushing times and sample dispersion when switching between chemistries.

Three different approaches are used in the RNM for designing reactor plates that give uniform residence time distribution. (a) Design for flow equipartition in the initial quadrant shape geometry by increasing the size of the reactant collecting channel to minimise its resistance (pressure drop). (b) Design for flow equipartition by modifying (to non-quadrant) the reaction plate geometry; however, a quadrant active region has to be used on a non-quadrant reactor plate for even residence time distribution. (c) Design for even residence time distribution by modifying the reactor plate geometry. The last approach utilises small collecting channels and the whole reactor plate, thus decreasing non-active areas on the reactor.

The flow fields in the different reactor plate geometries found from the resistance network model were also compared to the simulated ones by computational fluid dynamics. The numerical results confirmed even flow distribution in those geometries that had been designed for flow equipartition with RNM. For case (a) this also ensured even RDT on the reactor plate while for case (b) an active region on the reactor plate with quadrant shape

had to be used for even RDT. For the geometries designed for even residence time distribution (case (c)), however, numerical simulations of the flow field and particle tracking showed that the residence time distribution is not uniform across the reactor plate. This is because the assumption of straight streamlines in the RNM model used to define the shapes of these reactors is not valid. Geometries obtained via the resistance network model in this case are still a good first approximation to a final optimised geometry as results in Fig. 17 indicate. Particle tracking also confirmed the findings of the RNM that increased collecting channel volume and/or modified plate geometries can give uniform residence time distribution. Experimental observations of tracer injection into the mesh microreactor qualitatively confirmed the findings of the analytical and numerical models.

The above show that the simple analytical RNM can be applied to design plate type microstructures that give uniform flow and residence time distributions.

References

[1] C. Turner, J. Shaw, B. Miller, V. Bains, Solvent extraction using micro-mesh reactors, IMRET 4, Poster Session 1, Atlanta, 2000.

[2] C. Amador, P. Angeli, A. Gavriilidis, J. Shaw, D. Wenn, Analysis of mass transfer and chemical reaction in a mesh microreactor, in: Proceedings of the First International Symposium on Process Intensification and Miniaturisation (PIM-1), Newcastle, UK, August 18–21, 2003.

[3] C. Amador, P. Angeli, A. Gavriilidis, Flow distribution in microreactor scale-out geometries and the effect of manufacturing tolerances and channel blocking, Chem. Eng. J. 101 (2004) 379–390.

[4] O. Levenspiel, Chemical Reaction Engineering, Wiley, New York, 1972 (Chapter 9).

[5] H.S. Fogler, Elements of Chemical Reaction Engineering, 4th ed., Prentice-Hall, 2005.

[6] D.A. Wenn, J.E.A. Shaw, B. Mackenzie, A mesh microreactor for two-phase reactions, Lab Chip 3 (2003) 180–186.

[7] R.B. Bird, W.E. Stewart, E.N. Lightfoot, Transport Phenomena, Wiley, 2002.

[8] T.C. Papanastasiou, G.C. Georgiou, A.N. Alexandrou, Viscous Fluid Flow, CRC Press, 2000.

[9] FEMLAB Reference Manual, 2002.

[10] K.E. Johnson, private communication, 2004.

[11] R. Zitny, private communication, 2004.